# Correlation-based imaging of fast moving objects using a sparse network of passive receivers


Jacques Fournier
*Département de Mathématiques et Applications*
*École Normale Supérieure*
Paris, France
jacques.fournier@ens.fr

Josselin Garnier
*Centre de Mathématiques Appliquées*
*École Polytechnique*
Palaiseau, France
josselin.garnier@polytechnique.edu

George Papanicolaou
*Department of Mathematics*
*Stanford University*
Stanford, USA
papanicolaou@stanford.edu

Chrysoula Tsogka
*Applied Math unit*
*UC Merced*
Merced, USA
ctsogka@ucmerced.edu



***Abstract*—We consider the problem of imaging small fast moving objects. The imaging system consists of a powerful emitter (X-Band) located on the ground and several passive receivers. The study of imaging fast moving objects is motivated by the need to detect, track and image small energetic debris (1-10cm) revolving around the earth at a low orbit (200km-2000km). This is of interest because of the large amount of debris which substantially increases the risk of satellite damage from collisions. To determine the location and the velocity of the object we use correlation-based imaging because it has been shown to be robust to medium fluctuations such as atmospheric lensing and aberrations. We show that with only about 9 recording platforms we get as good a resolution as if we had a full $400 \times 400$ kilometer aperture.**



***Index Terms*—component, formatting, style, styling, insert**


## I. Introduction

The objective of this paper is to show that passive correlation based imaging with one or more emitters on the ground and several airborne receivers leads to hight resolution imaging of fast moving objects and therefore can be used for tracking and imaging satellites and small debris in LEO. This is of interest because there are roughly 700,000 debris of size larger than 1cm in LEO and there is concern that future collisions may have a chain reaction effect that would lead to an unacceptably risky environment [10], [11], [16].

The first results in this direction are presented in [5] (see schematic in Figure 1). The small fast moving object is modeled as a point-like reflector moving with constant velocity, $\boldsymbol{V}_T$. Debris are not necessarily in stable orbit but their motion follows Newton's law and therefore we seek to reconstruct the six unknowns that characterize their trajectories: the three components of the position and of the velocity. The imaging data are the scattered signals from a train of incident pulses emitted by a powerful transmitter located on the ground. The receivers in [5] are also assumed to be located on the ground and span an area of diameter $a$, which defines the physical aperture of the imaging system. Here we consider that the receivers are flying at altitude $h$ above the turbulent atmosphere, in which case we expect the correlation-based imaging method to be robust relative to atmospheric turbulence effects [7]–[9]. This is true for an imaging modality that uses receivers that are not located on the ground but are flying above the turbulent atmosphere, above the tropopause. The key idea is that passive correlation-based imaging becomes equivalent to having a virtual active array at the location of the passive receivers. By moving the receivers above the turbulent atmosphere, the atmospheric fluctuation effects on imaging are minimized and imaging resolution is as if we were in a homogeneous, fluctuation-free medium. We do not include in the simulations presented here turbulence effects. This will be

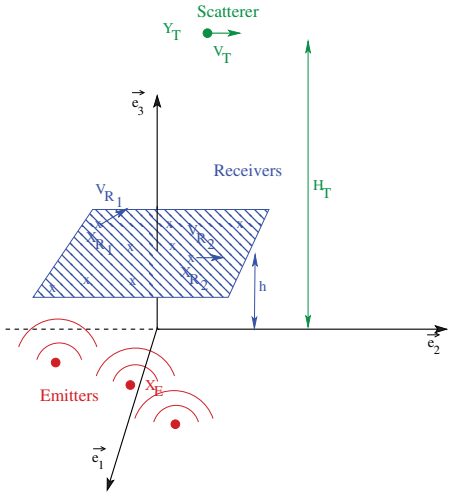


Fig. 1. Schematic of the imaging system's geometry. The receivers $R_1, R_2, \ldots, R_N$ are randomly placed in a domain of diameter $a$ at a fixed altitude $h$. The object to be imaged is moving with speed $\mathbf{V}_T$ at height $H_T$. On or more powerful transmitters $\boldsymbol{X}_E$ are located on the ground.


AFOSR FA9550-17-1-0238, AFOSR FA9550-18-1-0519.

considered in future work.

In synthetic aperture radar (SAR), a single airborne transmit/receive element is moving and its trajectory defines the synthetically created aperture of the imaging system [4], [6]. Analogously, the trajectory of the moving target defines an inverse synthetic aperture (ISAR) of length $T_{\rm tot}|\boldsymbol{V}_T|$, with $T_{\rm tot}$ the total recording time during the data gathering process. Other important parameters of the imaging system are the central frequency, $f_o$, and the bandwidth, $B$, which are determined by the emitter.

In this context, the well established matched-filter imaging method [3], [13] was studied and its performance was compared with a correlation-based imaging method. In matched-filter imaging the recorded signals are Doppler compensated as in [3], [12], [13] and synchronized with travel time delays so as to maximize the correlation with the emitted pulse, which is assumed known. The synchronization requires knowledge of the emitter location with high accuracy. Correlation-based imaging relies on cross correlations of signals between pairs of receivers. The signals are also Doppler compensated and synchronized, and must be recorded without down-ramping [1]. However, in this case the synchronization does not require knowledge of the emitter location since only time differences matter. For correlation-based imaging we do not need to know the pulse profile or the emission times but we need to record the whole train of scattered pulses. A sufficient high sampling rate is assumed so that the real-valued scattered signal can be recorded as in [1], [2].

A rigorous resolution analysis for both the matched-filter and the correlation-based imaging methods was carried out in [5] and it was shown that the two methods have similar resolution in cross-range. Cross-range is the coordinate that is orthogonal to the direction of the receivers/scatterer that defines the range. Note that it is the final resolution estimates that are comparable, while the computations for image formation in each case are quite different. The cross-range resolution estimate is $\lambda_o H_T/a$, with $H_T$ being the altitude of the moving target and $\lambda_o$ being the central wavelength. This is the well-known Rayleigh resolution formula. In the direction of the target's velocity, the ISAR aperture plays a role when it is big enough and the resolution estimate becomes $\lambda_o(\frac{H_T}{a} \wedge \frac{H_T}{2|\boldsymbol{V}_T|T_{\rm tot}})$ for the matched-filter, the wedge symbol, $\wedge$, means the minimum between the two quantities. In the range direction we see the biggest difference between the two methods: matched-filter resolution is $\frac{c_0}{2B}$ and relies on the bandwidth, while for the correlation-based imaging we obtain $\lambda_o \frac{H_T^2}{a^2}$. In correlation-based imaging range resolution does not depend on the bandwidth because the corresponding imaging function relies only on arrival-time differences. The resolution estimates for the velocity are given by the corresponding ones for the location divided by the recording time $T_{\rm tot}$. This is not true for the velocity estimate along the range direction provided by the matched-filter for which we obtain the extremely precise estimate $\frac{\lambda_o}{2T_{\rm tot}}$.

We illustrate here with numerical simulations that the resolution estimates obtained in the simplified configuration with the receivers located on the ground describe well the resolution that we obtain in the more realistic configuration considered here with moving receivers.

This paper is organized as follows. We begin with the data model and the problem setup in Section II. The two imaging methods are presented in Section III. In Section IV we present numerical simulations that verify our theoretical resolution estimates summarized in Tables II and III.

## II. Data model

We consider a (point) transmitter at $\boldsymbol{X}_E$ that emits a short pulse $f(t)$. The total field $u(t,\boldsymbol{x})$ is the solution of the wave equation

$$\frac{1}{c^2(t,\boldsymbol{x})}\frac{\partial^2 u}{\partial t^2} - \Delta u = f(t)\delta(\boldsymbol{x}-\boldsymbol{X}_E), \tag{1}$$

with a localized perturbation $\varrho_T$ centered at the moving target $\boldsymbol{X}_T(t)$,

$$\frac{1}{c^2(t,\boldsymbol{x})} = \frac{1}{c_0^2}\Big(1+\varrho_T\big(\boldsymbol{x}-\boldsymbol{X}_T(t)\big)\Big).$$

The incident field has the form

$$u^{(0)}(t,\boldsymbol{x}) = \frac{1}{4\pi\,|\boldsymbol{x}-\boldsymbol{X}_E|} f\Big(t-\frac{|\boldsymbol{x}-\boldsymbol{X}_E|}{c_0}\Big). \tag{2}$$

In the Born approximation, and for a small point-like scatterer, the scattered field is given by

$$u^{(1)}(t,\boldsymbol{x}) = -\frac{\rho}{c_0^2}\int_0^t d\tau G(t-\tau,\boldsymbol{x},\boldsymbol{X}_T(\tau))\,\frac{\partial^2 u^{(0)}(\tau,\boldsymbol{y})}{\partial\tau^2}\Big|_{\boldsymbol{y}=\boldsymbol{X}_T(\tau)}$$

where $\rho = \int \varrho_T(\boldsymbol{x})d\boldsymbol{x}$ is the reflectivity of the target and $G(t,\boldsymbol{x},\boldsymbol{y})$ denotes the Green's function. Using the expression for $u^{(0)}$ and integrating by parts twice we obtain the following expression for scattered field at the receiver at $\boldsymbol{x}=\boldsymbol{X}_R$

$$u_{{\rm s},R}(t) = -\frac{\rho}{c_0^2}\int_0^t d\tau \frac{1}{4\pi|\boldsymbol{X}_T(\tau)-\boldsymbol{X}_E|} f''\Big(\tau-\frac{|\boldsymbol{X}_T(\tau)-\boldsymbol{X}_E|}{c_0}\Big) \times \frac{1}{4\pi|\boldsymbol{X}_R-\boldsymbol{X}_T(\tau)|}\delta\Big(t-\tau-\frac{|\boldsymbol{X}_R-\boldsymbol{X}_T(\tau)|}{c_0}\Big).$$

We assume that the target is moving with constant velocity along the trajectory $\boldsymbol{X}_T(t)=\boldsymbol{Y}_T+\boldsymbol{V}_T t$, $t\in(-T_{\rm tot}/2, T_{\rm tot}/2)$ where $\boldsymbol{Y}_T$ denotes the location of the target at time 0. If we introduce

$$\Phi(\tau;t) = t-\tau-\frac{|\boldsymbol{Y}_T-\boldsymbol{X}_R+\tau\boldsymbol{V}_T|}{c_0},$$

then we have

$$\delta\left[\Phi(\tau;t)\right] = \frac{\delta[\tau-\tau(t)]}{|\partial_\tau\Phi(\tau(t);t)|},$$

with $\tau(t)$ the unique zero of $\tau\to\Phi(\tau;t)$ in $(0,t)$. Denoting $\boldsymbol{D}(t)=\boldsymbol{Y}_T-\boldsymbol{X}_R+t\boldsymbol{V}_T$, We find that $\tau(t)$ is given by

$$\tau(t) = t-\frac{|\boldsymbol{D}(t)|}{c_0\big(1-\big|\frac{\boldsymbol{V}_T}{c_0}\big|^2\big)}\left[\sqrt{1-\left|\frac{\boldsymbol{V}_T}{c_0}\right|^2+\left(\frac{\boldsymbol{V}_T}{c_0}\cdot\frac{\boldsymbol{D}(t)}{|\boldsymbol{D}(t)|}\right)^2} - \frac{\boldsymbol{V}_T}{c_0}\cdot\frac{\boldsymbol{D}(t)}{|\boldsymbol{D}(t)|}\right].$$

Using this in $u_{\mathrm{s},R}(t)$ we get the (model) signal recorded at the receiver

$$u_{\mathrm{s},R}(t) = -\frac{\rho f''\Big(\tau(t) - \frac{|\boldsymbol{X}_T(\tau(t)) - \boldsymbol{X}_E|}{c_0}\Big)}{(4\pi)^2 c_0^2 |\boldsymbol{X}_T(\tau(t)) - \boldsymbol{X}_E||\boldsymbol{X}_R - \boldsymbol{X}_T(\tau(t))|} \times \frac{1}{\Big|1 + \frac{\boldsymbol{V}_T}{c_0}\cdot\frac{\boldsymbol{D}(\tau(t))}{|\boldsymbol{D}(\tau(t))|}\Big|}.$$

## III. The imaging problem

Given the recorded signals $u_{\mathrm{s},R}(t)$ at various receiver locations $\boldsymbol{X}_R$, we seek to estimate the target's location $\boldsymbol{Y}_T$ and velocity $\boldsymbol{V}_T/c_0$ assumed to be small. This is a point in six dimensions in general. For satellites or debris in orbit it can be reduced to five with a "tangential" $\boldsymbol{V}_T$. We make here the assumption that the receiver locations are known. For matched field imaging the source location $\boldsymbol{X}_E$ must be also know with wavelength accuracy while for correlation based imaging we only need to know roughly the location of the source.

### A. Matched field imaging function

The idea behind the matched-filter imaging function is that we want to match the received signal with the emitted pulse. The matching process involves the assumed initial position and speed of the object $(\boldsymbol{Y}, \boldsymbol{V})$, and this matching can be shown to be maximal at the true position $(\boldsymbol{Y}_T, \boldsymbol{V}_T)$. The matching process takes into account $\gamma_{\mathrm{s}}$, a (derived) Doppler compensation factor,

$$\gamma_{\mathrm{s}}(\boldsymbol{X}, \boldsymbol{V}, \boldsymbol{X}_R) = 1 - \frac{\boldsymbol{V}}{c_0}\cdot\left(\frac{\boldsymbol{X} - \boldsymbol{X}_E}{|\boldsymbol{X} - \boldsymbol{X}_E|} + \frac{\boldsymbol{X} - \boldsymbol{X}_R}{|\boldsymbol{X} - \boldsymbol{X}_R|}\right).$$

The matched field imaging function is

$$\mathcal{I}^{\mathrm{MF}}(\boldsymbol{Y}, \boldsymbol{V}) = \frac{1}{N_E}\sum_{j=1}^{N_E}\mathcal{I}_j^{\mathrm{MF}}(\boldsymbol{Y} + \boldsymbol{V}S_j, \boldsymbol{V}),$$

$$\mathcal{I}_j^{\mathrm{MF}}(\boldsymbol{X}, \boldsymbol{V}) = \frac{1}{N}\sum_{R=1}^{N}\int dt\; u_{\mathrm{s},R}(S_j + t)\times f\Big(\gamma_{\mathrm{s}}(\boldsymbol{X}, \boldsymbol{V}, \boldsymbol{X}_R)\big(t - \frac{|\boldsymbol{X} - \boldsymbol{X}_R|}{c_0}\big) - \frac{|\boldsymbol{X} - \boldsymbol{X}_E|}{c_0}\Big)$$

This imaging function requires knowledge of the transmitter and receiver positions $\boldsymbol{X}_E$ and $\boldsymbol{X}_R$. We also need to know the pulse profile $f$. One wants to image a region around some point $\boldsymbol{Y}_T$, so the $j$-th scattered signal needs only to be recorded for a short time around $|\boldsymbol{Y}_T - \boldsymbol{X}_R|/c_0 + |\boldsymbol{Y}_T - \boldsymbol{X}_E|/c_0$.

### B. Cross correlation imaging function

We cross correlate the scattered signals recorded by pairs of receivers and migrate them with the appropriate Doppler compensation factors,

$$\mathcal{I}^{\mathrm{CC}}(\boldsymbol{Y}, \boldsymbol{V}) = \frac{1}{N_E}\sum_{j=1}^{N_E}\mathcal{I}_j^{\mathrm{CC}}(\boldsymbol{Y} + \boldsymbol{V}S_j, \boldsymbol{V}), \tag{3}$$

$$\mathcal{I}_j^{\mathrm{CC}}(\boldsymbol{X}, \boldsymbol{V}) = \frac{1}{N^2}\sum_{R,R'=1}^{N}\int u_{\mathrm{s},R}\left(S_j + \frac{t + t_s(\boldsymbol{X}, \boldsymbol{V}, \boldsymbol{X}_R)}{\gamma_{\mathrm{s}}(\boldsymbol{X}, \boldsymbol{V}, \boldsymbol{X}_R)}\right) \times u_{\mathrm{s},R'}\left(S_j + \frac{t + t_s(\boldsymbol{X}, \boldsymbol{V}, \boldsymbol{X}_{R'})}{\gamma_{\mathrm{s}}(\boldsymbol{X}, \boldsymbol{V}, \boldsymbol{X}_{R'})}\right) dt, \tag{4}$$

where $t_s(\boldsymbol{X}, \boldsymbol{V}, \boldsymbol{X}_R) = \frac{|\boldsymbol{X} - \boldsymbol{X}_E|}{c_0} + \gamma_{\mathrm{s}}(\boldsymbol{X}, \boldsymbol{V}, \boldsymbol{X}_R)\frac{|\boldsymbol{X} - \boldsymbol{X}_R|}{c_0}$. Now it is not necessary to know the pulse profile $f$, which could be different from one emission to another one. It is not necessary either to know the emission times with accuracy. But we need to record the whole train of scattered signals. Moreover correlation-based imaging has been shown to be robust to medium fluctuations when in a suitable imaging configuration [8].

Since the target is moving with large velocity, both matched filter and correlation-based imaging function must compensate for the Doppler factors, as in [12], [13] or [14], [15].

## IV. Numerical simulations

We assume that there is a single illuminating source on the ground, whose location need not be known for CC imaging. The emitted signals (synchronization, pulse form) are also not known. They are, however assumed known for MF imaging.

The recording platforms and randomly placed in a $400\times400$ kilometer square at a fixed altitude $h = 15$km. We consider here that the receivers are moving at different directions as illustrated in the schematic of Figure 2. The satellite flies in the $Y_2$ direction at constant speed starting right above the source on the ground.

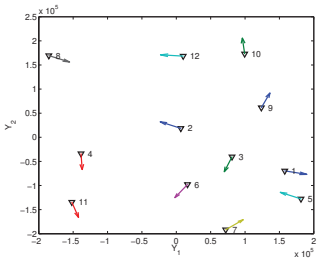


Fig. 2. Receiver distribution in a square with side $a = 400$ km. The black triangles denote the receiver locations at the beginning of the recordings and the arrows show the direction in which each receiver is moving. The labels correspond to each receiver's number, an integer from 1 to 12. The units are in km. The values of the parameters used in the numerical simulations are given in Table I.

The parameters for modeling SAR imagining of a fast moving small object with passive SAR on a platform above the atmosphere and microwave sources on the ground are given in Table I.

There are five "parameters" to be imaged: The three components of the scatterer's (say its initial) location and the (assumed) two components of its speed. We actually include

| System Parameters | | |
|---|---|---|
| Central Frequency | $f_0$ | 9.6 GHz |
| Bandwidth | B | 622 MHz |
| Number of Frequencies in Bandwidth | $N_f$ | 515 |
| Slow-time Sampling | $\Delta s$ | 0.015 s |
| Wave Speed | $c_0$ | $3 \times 10^8$ m/s |
| Central Wavelength | $\lambda_o$ | 3.12 cm |
| Altitude of Satellite | $H$ | 500 km |
| Speed of Satellite | $V_T$ | 7,610.6 m/s |
| Altitude of Drone | $h$ | 15 km |
| Velocity of Drone | $V_R$ | 50 m/s (180 km/hr) |

TABLE I
TYPICAL VALUES OF THE PARAMETERS FOR OUR IMAGING CONFIGURATION.

vertical speed as well since it is needed when dealing larger size space objects.

Each passive SAR receiver (drone) covers a distance of 1.1 km, in 22.5 secs. During this time the moving object covers a distance of 171 km. These are the recording windows used.

| | | **X-band** |
|---|---|---|
| $Y_1$ | $\frac{\lambda_o H_T}{a}$ | 3.75 cm |
| $Y_2$ | $\lambda_o(\frac{H_T}{a} \wedge \frac{H_T}{2V_T T_{\rm tot}})$ | 3.75 cm $\wedge$4.4 cm = 3.75 cm |
| $Y_3$ | $\frac{c_0}{2B} \wedge \lambda_o \frac{H_T^2}{2V_T T_{\rm tot} a}$ | 23 cm $\wedge$5.5 cm = 5.5 cm |
| $V_1$ | $\frac{\lambda_o H_T}{a T_{\rm tot}}$ | 0.17 cm/s |
| $V_2$ | $\frac{\lambda_o}{T_{\rm tot}}(\frac{H_T}{a} \wedge \frac{H_T}{2V_T T_{\rm tot}})$ | 0.17 cm/s $\wedge$0.19 cm/s = 0.17 cm/s |
| $V_3$ | $\frac{\lambda_o}{2T_{\rm tot}}$ | 0.07 cm/s |

TABLE II
MATCHED FILTER RESOLUTION ESTIMATES.

| | | **X-band** |
|---|---|---|
| $\boldsymbol{Y}_\perp$ | $\frac{\lambda_o H_T}{a}$ | 3.75 cm |
| $Y_3$ | $\lambda_o\Big(\frac{H_T^2}{a^2} \wedge \frac{2H_T^2}{aV_T T_{\rm tot}}\Big)$ | 4.7 cm $\wedge$22 cm = 4.7 cm |
| $\boldsymbol{V}_\perp$ | $\frac{\lambda_o H_T}{a T_{\rm tot}}$ | 0.17 cm/s |
| $V_3$ | $\frac{\lambda_o}{T_{\rm tot}}\Big(\frac{H_T^2}{a^2} \wedge \frac{2H_T^2}{aV_T T_{\rm tot}}\Big)$ | 0.2 cm/s $\wedge$1 cm/s = 0.2 cm/s |

TABLE III
CORRELATION-BASED IMAGING RESOLUTION ESTIMATES.

The theoretical imaging resolution formulas are given in Table II for MF and in Table III for CC imaging. We also give in the tables the resolution estimates for the two imaging methods in the X-band and the S-band regimes.

The images obtained using MF and CC are shown in Figures 3 and 4. The numerical results are in very good agreement with the theoretical resolution estimates. Remark that the theoretical estimates are obtained for the case of stationary receivers located on the ground while in our numerical simulations the receivers are flying at altitude $h = 15$km. Since the location of the receivers is assumed known their movement should not affect the resolution. This is confirmed by the simulations.

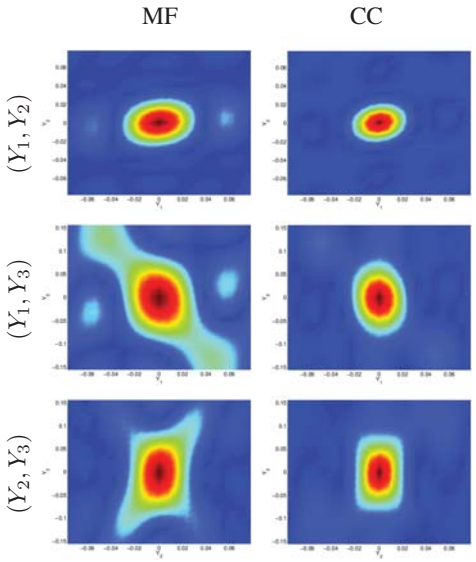


Fig. 3. Location reconstruction. Images with MF and CC in the $(Y_1, Y_2)$ plane (top), the $(Y_1, Y_3)$ plane (center) and $(Y_2, Y_3)$ plane (bottom). The units are in m. The moving object's velocity is $V_T = 7610$m/s. The recording duration is $T_{\rm tot} = 22.5$s.

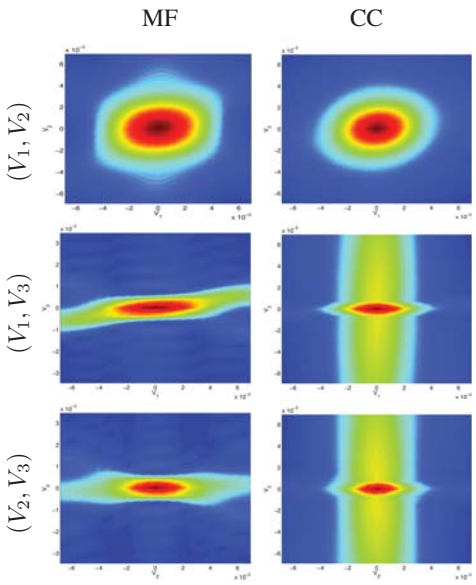


Fig. 4. Velocity reconstruction. Images with MF and CC in the $(V_1, V_2)$ plane (top), the $(V_1, V_3)$ plane (center) and $(V_2, V_3)$ plane (bottom). The units are in m/s. The moving object's velocity is $V_T = 7610$m/s. The recording duration is $T_{\rm tot} = 22.5$s.

To examine how the number of receivers used affects the imaging results we show in Figure 5 the images obtained using subsets of receivers with cardinality $4$, $6$, $9$, and $12$. For each number of receivers used we selected the receiver set so that they span the whole square aperture (see Figure 2) as best as possible given our initial set of 12 receivers. We made the following choices: when using $\mathbf{4}$ receivers we selected the receivers with labels $5$, $8$, $10$ and $11$. Let us denote the receiver set $\mathcal{S}^4 = \{5, 8, 10, 11\}$. Then we increased the number of receivers to $\mathbf{6}$ by adding receivers 7 and 12, so that $\mathcal{S}^6 = \{5, 7, 8, 10, 11, 12\}$. In the case of $\mathbf{9}$ receivers we took $\mathcal{S}^9 = \{2, 4, 5, 7, 8, 9, 10, 11, 12\}$ and $\mathcal{S}^{12}$ is the set containing all available receivers.

The images shown in figure 5 are the $\mathcal{I}^{\mathrm{MF}}(\boldsymbol{Y}, \boldsymbol{V})$ and $\mathcal{I}^{\mathrm{CC}}(\boldsymbol{Y}, \boldsymbol{V})$ images in the plane $(Y_1, Y_2)$ obtained using the receiver sets $\mathcal{S}^4$, $\mathcal{S}^6$, $\mathcal{S}^9$, and $\mathcal{S}^{12}$ from top to bottom respectively. We observe that the quality of both MF and CC images increases rapidly with the number of receivers and very good results are obtained using just $9$ receivers. For all considered configurations, we observed that the resolution of the images is stable and does not vary significantly with the number of receivers used. It is mainly the side-lobes that are affected by the number of receivers used. We presented here results only for the location variables in the plane $(Y_1, Y_2)$. However, similar results (not shown here) are obtained for the other unknowns.

We have shown that passive SAR imaging of satellites can be done with a resolution that is essentially the optimal one, properly interpreted, when using a suitably adjusted imaging function to account for rapid target motion. The resolution theory is challenging but essentially complete now, both for CC and MF (currently used) imaging. CC and MF imaging resolutions are comparable for multiple receivers (continuum approximation) and "large" apertures [2], [5].

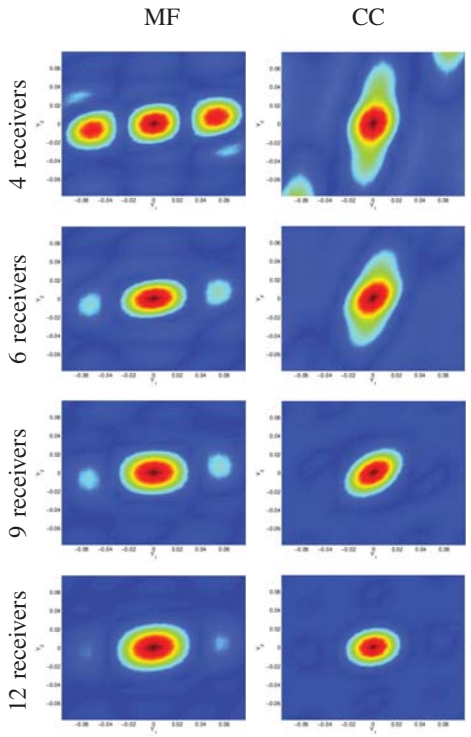


Fig. 5. Cross-section of the image in the plane $(Y_1, Y_2)$ obtained using 4, 6, 9, and 12 moving receivers respectively. Images with MF (left column) and CC (right column). The abscissa is for $Y_1$ and the ordinate for $Y_2$. The units are in m.

## REFERENCES


[1] *IEEE Aerospace and Electronic Systems Magazine*, 27, 2012.

[2] L. Borcea, J. Garnier, G. Papanicolaou, K. Solna, and C. Tsogka. Resolution analysis of passive synthetic aperture imaging of fast moving objects. *SIAM J. Imaging Sciences*, 10(2):665–710, 2017.

[3] M. Cheney and B. Borden. Imaging moving targets from scattered waves. *Inverse Problems*, 24:1–22, 2008.

[4] J. C. Curlander and R. N. McDonough. *Synthetic aperture radar*. Wiley, 1991.

[5] J. Fournier, J. Garnier, G. Papanicolaou, and C. Tsogka. Matched-filter and correlation-based imaging for fast moving objects using a sparse network of receivers. *SIAM J. Imaging Sciences*, 10(4):2165–2216, 2017.

[6] G. Franschetti and R. Lanari. *Synthetic aperture radar processing*. Boca Raton, FL: CRC Press, 1999.

[7] J. Garnier and G. Papanicolaou. Correlation based virtual source imaging in strongly scattering media. *Inverse Problems*, 28:075002, 2012.

[8] J. Garnier and G. Papanicolaou. *Passive imaging with ambient noise*. Cambridge University Press, 2016.

[9] J. Garnier, G. Papanicolaou, A. Semin, and C. Tsogka. Signal-to-noise ratio analysis in virtual source array imaging. *SIAM J. Imaging Sciences*, 8:248–279, 2015.

[10] J. A. Haimerl and G. P. Fonder. Space fence system overview. In *Proceedings of the Advanced Maui Optical and Space Surveillance Technology Conference*, 2015.

[11] D. Mehrholz, L. Leushacke, W. Flury, R. Jehn, H. Klinkrad, and M. Landgraf. Detecting, tracking and imaging space debris. *ESA Bulletin*, 109:128–134, 2002.

[12] S. V. Tsynkov. On the use of start-stop approximation for spaceborne sar imaging. *SIAM J. Imaging Sciences*, 2:646–669, 2009.

[13] L. Wang, M. Cheney, and B. Borden. Multistatic radar imaging of moving targets. *IEEE Trans. Aerosp. Electron. Syst.*, 48(1):230–242, 2012.

[14] L. Wang, C. E. Yarman, and B. Yazici. Doppler-hitchhiker: A novel passive synthetic aperture radar using ultranarrowband sources of opportunity. *IEEE Transactions on Geoscience and Remote Sensing*, 49:3521–3537, 2011.

[15] L. Wang, C. E. Yarman, and B. Yazici. Theory of passive synthetic aperture imaging, in excursions in harmonic analysis. *Applied and Numerical Harmonic Analysis*, 1:211–236, 2013.

[16] K. Wormnes, R. Le Letty, L. Summerer, R. Schonenborg, O. Dubois-Matra, E. Luraschi, A. Cropp, H. Kragg, and J. Delaval. Esa technologies for space debris remediation. In *Proceedings of 6th European Conference on Space Debris, Darmstadt, Germany*, 2013.